A&A 573, A92 (2015)
DOI: 10.1051/0004-6361/201424393

Astronomy & Astrophysics

The Na-O anticorrelation in horizontal branch stars

V. NGC 6723⋆,⋆⋆

R. G. Gratton[1], S. Lucatello[1], A. Sollima[2], E. Carretta[2], A. Bragaglia[2], Y. Momany[1,3], V. D'Orazi[4,5], M. Salaris[6], S. Cassisi[7,8], and P. B. Stetson[9]

[1] INAF – Osservatorio Astronomico di Padova, Vicolo dell'Osservatorio 5, 35122 Padova, Italy
e-mail: raffaele.gratton@oapd.inaf.it
[2] INAF – Osservatorio Astronomico di Bologna, via Ranzani 1, 40127 Bologna, Italy
[3] European Southern Observatory, Alonso de Cordova 3107, Vitacura, Santiago, Chile
[4] Department of Physics & Astronomy, Macquarie University, Balaclava Rd., North Ryde, Sydney, NSW 2109, Australia
[5] Monash Centre for Astrophysics, School of Mathematical Sciences, Building 28, Monash University, VIC 3800, Australia
[6] Astrophysics Research Institute, Liverpool John Moores University, IC2, Liverpool Science Park, 146 Brownlow Hill, Liverpool L3 5RF, UK
[7] INAF – Osservatorio Astronomico di Teramo, via Collurania, 24100 Teramo, Italy
[8] Instituto de Astrofisica de Canarias, La Laguna, 38205 Tenerife, Spain
[9] Dominion Astrophysical Observatory, Herzberg Institute of Astrophysics, National Research Council, 5071 West Saanich Road, Victoria, British Columbia V9E 2E7, Canada

Received 13 June 2014 / Accepted 22 October 2014

ABSTRACT

We used FLAMES+GIRAFFE (Medusa mode) at the VLT to obtain moderately high resolution spectra for 30 red horizontal branch (RHB) stars, 4 RR Lyrae variables, and 17 blue horizontal branch (BHB) stars in the low-concentration, moderately metal-rich globular cluster NGC 6723 ([Fe/H] = −1.22 ± 0.08 from our present sample). The spectra were optimized to derive O and Na abundances. In addition, we obtained abundances for other elements, including N, Fe, Mg, Ca, Ni, and Ba. We used these data to discuss the evidence of a connection between the distribution of stars along the horizontal branch (HB) and the multiple populations that are typically present in globular clusters. We found that all RHB and most (13 out of 17) BHB stars are O-rich, Na-poor, and N-poor; these stars probably belong to the first stellar generation in this cluster. Only the four warmest observed stars are (moderately) O-poor, Na-rich, and N-rich, and they probably belong to the second generation. While our sample is not fully representative of the whole HB population in NGC 6723, our data suggest that in this cluster only HB stars warmer than ∼9000 K, that is one fourth of the total, belong to the second generation, if at all. Since in many other clusters this fraction is about two thirds, we conclude that the fraction of first/second generation in globular clusters may be strongly variable. In addition, the wide range in colour of chemically homogeneous first-generation HB stars requires a considerable spread in mass loss (>0.10 $M_{\odot}$). The reason for this spread is yet to be understood. Finally, we found a high Ba abundance, with a statistically significant radial abundance gradient.

Key words. stars: abundances – stars: Population II – globular clusters: general – globular clusters: individual: NGC 6723 – stars: evolution

1. Introduction

The horizontal branch (HB) of globular clusters (GCs) is the locus in their colour-magnitude diagram (CMD) that contains the stars that are burning He in their cores. The initial location of the stars on the HB (the zero-age horizontal branch, ZAHB) is expected to depend primarily on their mass and chemical composition; while still burning helium in their cores, the stars experience limited changes in surface temperature and luminosities; they become much redder and brighter only in very late stages of the HB phase when very little He is left in their cores. Until recently, GCs were considered to be simple stellar populations, that is, all stars were thought to have the same age and chemical composition. Following that scheme, we expect that HB stars have a colour distribution due only to their evolution off the ZAHB, unless they loose different amounts of mass while still on the red giant branch (RGB). However, it was immediately clear from the first quantitative comparison between models and data several decades ago that, in each GC, stars distribute over a range in colour much wider than expected from this simple evolutionary consideration, with considerable variation in this range for different clusters (see, e.g., Rood 1973). In addition, it is also known that median colours of the HB stars in different clusters – originally assumed to be coeval – are not simply a function of metallicity, as originally expected based on evolutionary models (see Faulkner 1966). These two facts constitute the "second parameter" problem (Sandage & Wildey 1967; van den Bergh 1967). Many different explanations have been suggested for this phenomenon (for reviews, see Fusi Pecci & Bellazzini 1997; Catelan 2009). In the past few years, it has become clear that most of the complex phenomenology can be explained by a combination of different factors: cluster-to-cluster age differences, metallicity-dependent mass loss with small but not negligible star-to-star variations, and star-to-star variations

⋆ Based on observations collected at ESO telescopes under programme 087.D-0230.
⋆⋆ Tables 2, 3, 5, 7, and 8 are available in electronic form at http://www.aanda.org

in the He abundances related to the multiple population phenomenon (Gratton et al. 2010; see also Dotter 2013; Milone et al. 2014). In addition, other factors (binarity, variation of the total CNO content, and perhaps rotation; see e.g. Rood 1973) should also be considered, at least for some specific clusters. Moreover, the relative role of the star-to-star variations in mass loss and in chemical composition is yet to be determined.

This complex problem can be attacked following a variety of approaches, including statistical analyses of large samples of GCs or studies of the properties of the variable stars, for instance. Basic information can be obtained by determining the chemical composition of stars in different locations along the HB. In fact, we expect that evolved He-rich stars (belonging to the so-called second generation in GCs, SG; Gratton et al. 2012a) have masses lower than He-normal ones (members of the first generation, FG), and they should occupy a bluer location on the HB (see Ventura et al. 2001; D'Antona et al. 2002; Piotto et al. 2005; Cassisi et al. 2013, following the earlier suggestions by, e.g., Rood 1973; Norris et al. 1981). When the He abundances of the individual HB stars are known, synthetic HB populations can be compared with observed distributions of stars along the HB, allowing determination of the residual scatter in mass that can be attributed to other factors.

While conceptually simple, this method has several limitations. He abundances are difficult to derive directly because He lines are very weak in cool stars ($T_{\rm eff} < 9000$ K) and because stars warmer than the so-called Grundahl jump (at about $T_{\rm eff} \sim 11\,500$ K; Grundahl et al. 1999) do not have an outer convective envelope. In such warm stars, sedimentation and radiative levitation strongly affect the composition of the atmosphere, making it not feasible to deduce the original stellar composition. On the other hand, we may use elements other than He as useful diagnostics of the multiple population phenomenon for stars cooler than the Grundahl jump. Very useful information can be obtained using Na and O lines: while the relation between the abundances of these elements and that of He is probably not linear (Ventura & D'Antona 2008; Decressin et al. 2007), large He abundances in SG stars are always accompanied by a large overabundance of Na and deficiency of O with respect to the composition of He-normal FG stars of the same cluster. Stars on the blue end of the HB of a cluster are then expected to be richer in Na and N, and poorer in O, than stars at the red end.

First attempts to use this approach for a better understanding of the HB morphology have been the studies by Villanova et al. (2009), Marino et al. (2011), and Villanova et al. (2012) on a few HB stars in NGC 6752 and M 4. The results from these abundance analyses agreed in general with the hypothesis that the spread along the HB in these clusters is mostly determined by variations of He abundances among the multiple populations present in these clusters. On the other hand, other studies based on pulsational properties of RR Lyrae variables, for instance, show that the situation might be more complex because at least for some clusters, such as M 3, there seems to be no evidence for variation of He, at least close to the instability strip (see discussion in Catelan et al. 2009, and references therein). To further enlarge the small sample of clusters with an extensive abundance analysis of HB stars, we started a small survey of seven GCs; results for five of them have already been published: NGC 2808 (Gratton et al. 2011), NGC 1851 (Gratton et al. 2012b), 47 Tuc and M 5 (Gratton et al. 2013), and M 22 (Gratton et al. 2014). In this paper we present the results for a sixth cluster, NGC 6723, while those for the last one (NGC 6388) will be presented in a future paper. In the meantime, other studies on this same subject appeared and included the analysis of HB stars in M 22 (Marino et al. 2013) and NGC 6397 (Lovisi et al. 2012). The pattern emerging from all these studies generally confirms the scenario of the multiple populations, although at least for M 5 some additional mechanism should be considered.

NGC 6723 was selected for this analysis because it has an HB quite extended in colour, ranging from stars redder than the RR Lyrae instability strip to stars bluer than the Grundahl jump, similar to M 5. The large extension in colours over a range where the abundance analysis may still provide useful results makes it a suitable cluster on which to test the physical mechanism causing the spread in mass of HB stars. The overall properties of NGC 6723 can clearly be estimated from accurate HST photometric studies because this cluster was included both in the snapshot survey by Piotto et al. (2002) and in the more recent ACS survey by Sarajedini et al. (2007). The papers by Sollima et al. (2007) and Milone et al. (2012), also using HST, were dedicated to a search for binaries in the cluster core. Unfortunately, these photometric studies either focused on the central part of the cluster or on the main-sequence stars; hence there is little overlap with the HB stars that we observed in our spectroscopic study. Recent ground-based photometric studies have been performed by Stetson (in prep.) and by Lee et al. (2014). We extensively used these photometric data in our analysis. NGC 6723 has a low reddening ($E(B-V) = 0.05$), a low concentration ($c = 1.11$), and a reasonably small distance modulus ($(m-M)_V = 14.84$), which all facilitate the analysis. Its overall luminosity ($M_V = -7.84$; all these values are taken from the compilation of data for GCs made by Harris 1996, as downloaded from the internet in February 2014) is somewhat above the average for galactic GCs. Like M 4 and M 5, NGC 6723 is a moderately metal-rich cluster: determinations of its metallicity include values of [Fe/H] $= -1.26 \pm 0.09$ from high-dispersion spectroscopy of three red giants by Fullton & Carney (1996), -1.14 from the colour-magnitude diagram and integrated spectrophotometry (Zinn & West 1984), -1.09 by DDO photometry (Smith & Hesser 1986), -1.35 from Washington photometry (Geisler 1986), [Fe/H] $= -1.23 \pm 0.11$ from a Fourier analysis of the light curves of RR Lyrae variables (Lee et al. 2014), and -1.09 ± 0.14 from the Ca triplet (Rutledge et al. 1997). Note that almost all these values are lower than the values of [Fe/H] $= -1.10$ quoted by Harris (1996, 2010 edn.). None of these studies was aimed at studying multiple populations in this cluster. NGC 6723 is a very old cluster according to several age determinations (Marín-Franch et al. 2009; Dotter et al. 2010; VandenBerg et al. 2013); in this respect, NGC 6723 is similar to M 4 and it looks older than M 5. The mean period of the RR Lyrae stars places this cluster in the Oosterhoff I group (see Lee et al. 2014). Finally, the orbit of NGC 6723 makes it a member of the inner halo (Dinescu et al. 2003), although it is projected quite close to the Galactic bulge. On the whole, NGC 6723 appears to be a quite typical moderately metal-rich GC, its main peculiarity being the low concentration. Unfortunately, no previous extensive study of Na and O abundances along the RGB exist for this cluster. The anomalous extension of the HB of NGC 6723 with respect to that of NGC 6171, for example, which has a similar metallicity, was noticed several decades ago (see Smith & Hesser 1986). Gratton et al. (2010) briefly discussed this cluster: they showed that the colour distribution along the HB looks bimodal, and it cannot be reproduced by a single Gaussian distribution in mass. At the time, this was considered evidence for the presence of multiple populations.

Section 2 presents the observations and data reduction, explaining how they differ from what has been done for the other GCs studied in this series, and briefly discusses radial and

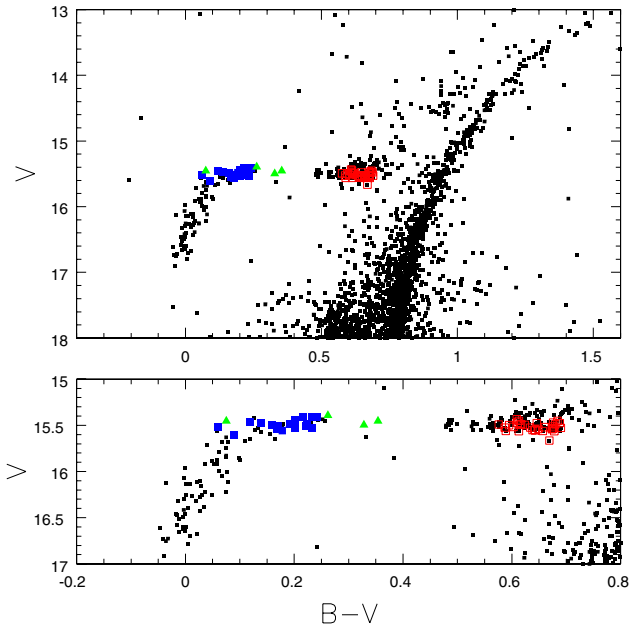

Fig. 1. *Upper panel*: ($V, B-V$) colour–magnitude diagram of NGC 6723 from Lee et al. (2014). *Lower panel*: blow-up of the HB region. Stars selected for observations are marked with large symbols: filled blue squares are BHB stars, open red squares are RHB stars, and filled green triangles are RR Lyrae variables.

rotational velocities determined from our spectra. We derive the atmospheric parameters and provide details of the abundance analysis in Sect. 3. Section 4 presents the results of this analysis. Finally, in Sect. 5 we compare the composition of NGC 6723 with that of other GCs and compare the distribution of stars along the HB with that of synthetic populations specifically constructed for this purpose.

2. Observations

We observed a total of 58 candidate HB stars of NGC 6723 with FLAMES + GIRAFFE at the VLT (Pasquini et al. 2004). The instrument was used in MEDUSA mode, with fibres pointing to each star and several (∼20) fibres used for determining the local sky background. The stars were selected from the *BVI* photometry by Stetson (in prep.; see Fig. 1); the field coverage is 100% complete out to a radius of 16 arcmin, and partial to a radius of 35 arcmin from the centre of the cluster; for comparison, the farthest member star of NGC 6723 in our spectroscopic sample is at 7.35 arcmin from the center. We selected for observation stars on the RHB[1] and on the BHB of the cluster, avoiding those with $V > 15.6$ because these stars are probably warmer than the Grundahl jump. We also tried to avoid placing fibres on stars within the instability strip because our observations (scheduled in service mode) were not optimized for variable stars. However, as reported below, four RR Lyrae stars were actually observed because they were erroneously recorded out of the instability strip in the photometry by Stetson (in prep.), which used observations made at only a few epochs. Only uncrowded stars were selected, that is, those without any contaminant with a V magnitude brighter than $V_* + 2$ within 2 arcsec from it; here V_* is the magnitude of the programme star. For this reason and to avoid fiber-to-fiber collisions, the star closest to the cluster center is at 0.98 arcmin. Seven of the observed stars (all close to the RHB of the cluster in the colour-magnitude diagram) were not members of NGC 6723 because they have discrepant radial velocities and abundances. These non-members were typically projected at large distances from the cluster center, but still within the tidal radius. Of the remaining 51 bona-fide members of NGC 6723, 17 are BHB stars, 30 are RHB stars, and the remaining four are RR Lyrae variables according to cross-identification with the list by Lee et al. (2014). The UVES fibres were used to acquire spectra of stars on the asymptotic giant branch of the cluster; they will be analysed in a future paper.

Table 1. Observing log.

Set up HR	Date	UT Start	Exp. time (s)	Airmass	Seeing (arcsec)
12	2011-07-11	07:14:23.5	2800	1.263	2.18
12	2011-08-27	00:10:09.5	2800	1.061	1.32
19	2011-07-18	06:03:41.7	2800	1.145	0.80
19	2011-07-18	06:52:18.1	2800	1.282	0.58

As was the case for the observations of the other GCs of this series, we used two set-ups: HR12 (wavelength range 5821−6146 Å, resolution $R \sim 18\,700$), and HR19A (wavelength range 7745−8335 Å, resolution $R \sim 13\,867$), allowing observation of the Na D doublet and the O I triplet at 7771−74 Å. These are the strongest features due to Na and O in the spectra of HB stars that are accessible from the ground. We aimed to obtain a final $S/N = 50$ per pixel. The observations (see Table 1) were carried out in service mode. The first frame with the HR12 set-up was acquired in poor observing conditions, yielding spectra with a S/N markedly lower than the other exposures (see Cols. 2−5 of Table 3). We used these data only to derive radial velocities (see Cols. 6−9 of the same table), the abundance analysis is based on the remaining spectra.

Photometric data for the programme stars are listed in Table 2. It includes the *BV* photometry by Stetson (in prep.), as well as the high quality *BV* photometry by Lee et al. (2014), kindly provided by the first author of that paper. In addition, we also listed the JHK_S photometric data from the 2MASS catalogue (Skrutskie et al. 2006). Since the observed stars are not in the inner region of the cluster, the WFPC2 photometry of Piotto et al. (2002) is of little help. We also searched for stars in common with the ACS photometry by Sarajedini et al. (2007), but we could not cross-identify any star because the observed stars are brighter than those listed in that catalogue.

Spectra were reduced using the ESO GIRAFFE pipeline, which provides wavelength-calibrated spectra. Sky subtraction was performed using IRAF[2]. We selected not to sum the individual spectra, but rather to measure velocities and equivalent widths on each of them, and then averaged the results of the analysis. The values from individual spectra are labelled as A and B in Table 3.

Telluric absorption lines were removed from the HR19A spectra by dividing them by an average spectrum of a few

[1] The RHB stars selected for observation have $15.445 < V < 15.560$ on the original photometry used for selection. There is then a bias against brighter RHB stars, although membership in the cluster of all these brighter stars is to be demonstrated. In principle, these stars might be He-rich, but if they are He-rich, they should also be massive to be on the RHB. Most likely, these stars are simply He-normal stars evolved off the ZAHB, as shown by the simulations presented below.

[2] IRAF is distributed by the National Optical Astronomy Observatory, which is operated by the Association of Universities for Research in Astronomy (AURA) under cooperative agreement with the National Science Foundation.

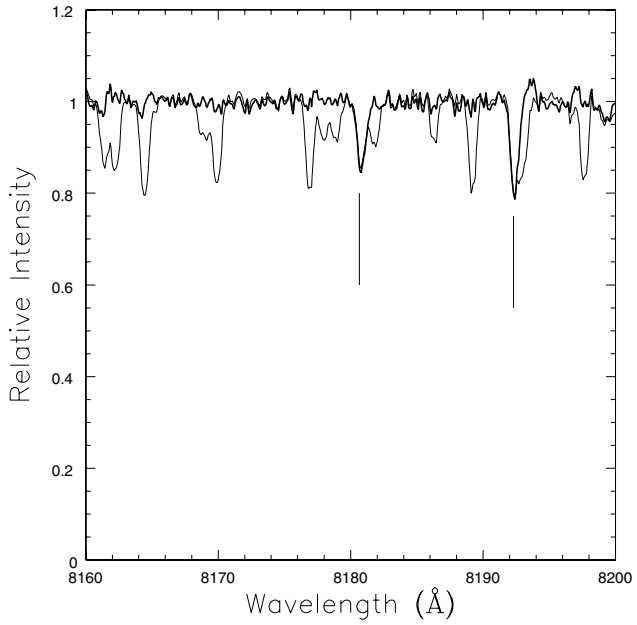

Fig. 2. Example of subtraction of telluric lines from the spectra obtained with the HR19A set-up following the procedure described in the text (thin line: before division; thick line: after division). The marks indicate the Na doublet at 8183−94 Å, slightly shifted blueward due to the geocentric radial velocity of the star (#32170) at the epoch of observation.

extreme BHB stars in NGC 1851 (Gratton et al. 2012b). Figure 2 shows an example of such a subtraction. We deem this subtraction to be fully satisfactory.

2.1. Radial velocities

As mentioned above, radial velocities were measured on the individual spectra using a few selected lines. Average radial velocities and the rms scatter around them are given in Cols. 10 and 11 of Table 3. The average value over all stars (excluding the RR Lyrae variables) is -95.8 ± 0.6 km s^{-1}, with an rms scatter for individual stars of 4.4 km s^{-1}. The median value of the rms scatter from different measurements for an individual star is about 1 km s^{-1}, which is much smaller than the star-to-star scatter. For comparison, Harris (1996, 2010 edn.) listed an average velocity for NGC 6723 of -94.5 ± 3.6 km s^{-1}, in good agreement with our determination, considering the large errors and scatter of the individual values from which this result is obtained (Zinn & West 1984: -90 ± 20 km s^{-1}; Hesser et al. 1986: -79 ± 7 km s^{-1}; Rutledge et al. 1997: -100.3 ± 9.9 km s^{-1}). The rms scatter we obtained implies an internal velocity dispersion of 4.3 km s^{-1}, which represents the first measure of this quantity in NGC 6723. We note here that the stars we observed are at a largest/smallest projected distance from the cluster center of 0.98/7.35 arcmin, with a median value of 2.3 arcmin. For comparison, the core, tidal, and half-light radii of NGC 6723 are 0.83, 13.7, and 1.53 arcmin, respectively (data from Harris 1996). Our data then refer to the outer regions of the cluster.

We found a small systematic difference when we considered BHB and RHB stars separately. The average radial velocities are -94.5 ± 0.8 km s^{-1} for BHB and -96.4 ± 0.9 km s^{-1} RHB stars. The difference (1.9 ± 1.2 km s^{-1}) is only marginally significant. If real, it might indicate a highest convective blue-shift for the RHB stars with respect to the BHB. Trying to better establish this point, we considered all those clusters for which we have radial velocities from both BHB and RHB stars from this survey. In addition to NGC 6723, we have data for three other clusters: NGC 1851, NGC 2808, and M 5, for which we found radial velocity differences of 1.9 ± 0.9, 7.8 ± 4.0, and 1.4 ± 1.0 km s^{-1}, respectively. In all cases, the offset is in the sense that the radial velocities for BHB stars are higher than those for RHB. The weighted average of all these data is 1.9 ± 0.6 km s^{-1}. The offset is significant at more than 3σ. Since we expect no real systematic difference in the average velocities of BHB and RHB stars, we assume that this effect is due to systematic errors in the measurements. Given that the same lines are used for the two sets of stars, we suggest that RHB stars have a convective blue-shift higher than the BHB stars (note that Na D lines have quite a strong weight in our radial velocities). Regardless of its cause, this effect should be considered before combining data from stars in these evolutionary phases for dynamical analysis of the clusters.

Finally, there is no strong indication favouring intrinsic variability of the radial velocities for any of the non-variable stars we observed, although our data are certainly not ideal for detecting spectroscopic binaries. On the other hand, quite large variations were obtained for three of the four RR Lyrae variables we observed.

2.2. Rotational velocities

It is well known that a fraction of the BHB stars rotate at moderate velocity (up to several tens km s^{-1}; Peterson 1983; Behr et al. 1999; Recio-Blanco et al. 2004). Generally, fast rotators are found only among BHB stars cooler than the Grundhal jump (Behr 2003a; Recio-Blanco et al. 2004; Lovisi et al. 2012); only a few RHB stars have been found to rotate (Behr et al. 2003b) and most likely they result from the evolution in close binary systems (see the case of a fast rotator in M 5 discussed in Gratton et al. 2013). We call the stars with $V \sin i > 20$ km s^{-1} fast rotators. We may use our spectra to search for fast rotators among the BHB stars we are observing in NGC 6723 (none of the RHB stars have lines wider than expected from instrumental effects). Since other lines are weak, we obtained the full width at half maximum (FWHM) of the O I spectral lines. They are given in Col. 12 of Table 3, along with their uncertainties as estimated from the scatter of individual measurements (Col. 13). They were transformed to rotational velocities following the same method as described in Gratton et al. (2014). As in that paper, whenever a lower value was obtained, we assumed an upper limit of 5 km s^{-1}. Most stars are slow rotators ($v \sin i < 10$ km s^{-1}); only three stars rotate at moderate speed, but none is a fast rotator according to the previous definition. This result is clearly at odds with what we recently obtained for the BHB stars in M 22, where we found 34 fast rotators among 92 stars (Gratton et al. 2014).

More in general, the fraction of fast rotators among BHB stars (here, only stars cooler than the Grundahl jump are considered) seems to be a function of the cluster metallicity and of the HB colour as represented by the HBR index[3]. Table 4 collects data available for 15 GCs. We also list [Fe/H] values and HBR ratios from Harris (1996, 2010 edn.). These data were used to construct Fig. 3, where we plot the fraction of fast rotators among BHB stars as a function of [Fe/H]. The highest percentages of fast rotators (30−70%) are obtained for moderately metal-poor clusters (NGC 6397, M 22, M 13, and M 79) that typically have very blue HBs. A lower percentage

[3] HBR is defined as $[n(\mathrm{BHB}) - n(\mathrm{RHB})]/[n(\mathrm{BHB}+n(\mathrm{RR})+n(\mathrm{RHB})]$, where n(BHB), n(RHB), n(RR) are the number of HB stars bluer than, redder than, and within the instability strip, respectively.

Table 4. Fraction of fast rotators ($V \sin i > 20$ km s^{-1}) among BHB stars cooler than the Grundahl jump.

NGC	Messier	[Fe/H]	HBR	N(BHB)	N(Fast)	Source
6341	M 92	–2.35	0.91	22	7	Behr (2003a)
7078	M 15	–2.33	0.67	25	3	Recio-Blanco et al. (2004)
						Behr et al. (2000b)
						Behr (2003a)
4590	M 68	–2.27	0.17	11	3	Behr (2003a)
6397		–1.98	0.98	40	23	Lovisi et al. (2012)
6093	M 80	–1.75	0.93	7	0	Recio-Blanco et al. (2004)
6656	M 22	–1.70	0.91	92	34	Gratton et al. (2014)
6205	M 13	–1.58	0.97	28	8	Behr et al. (2000a)
						Behr (2003a)
1904	M 79	–1.58	0.89	12	7	Recio-Blanco et al. (2004)
5272	M 3	–1.50	0.08	28	3	Behr (2003a)
5904	M 5	–1.33	0.31	44	5	Gratton et al. (2013)
288		–1.32	0.98	16	0	Behr (2003a)
6723		–1.22	–0.08	17	0	This paper
1851		–1.18	–0.36	27	1	Gratton et al. (2012b)
6121	M 4	–1.18	–0.06	6	0	Villanova et al. (2012)
2808		–1.18	–0.49	9	0	Recio-Blanco et al. (2004)

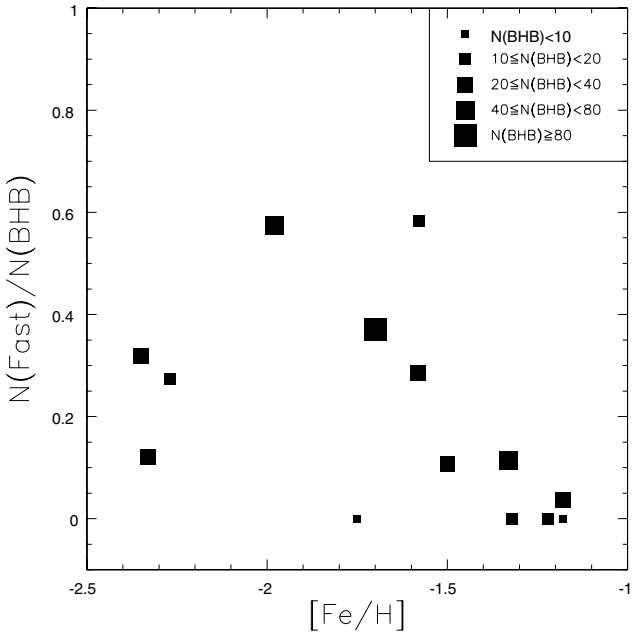

Fig. 3. Fraction of fast rotators ($V \sin i > 20$ km s^{-1}) among BHB stars as a function of cluster [Fe/H] value. Symbol size represents the number of stars that have been examined in the different clusters.

of between 10–30% is obtained for the most metal-poor clusters (M 92, M 15, and M 68), which are typical Oosterhoff II clusters. Fast rotators are rare among BHB stars in metal-rich clusters ([Fe/H] > −1.3). Most of these last clusters are Oosterhoff I clusters. However, fast rotators are also absent from the BHB stars of the metal-rich cluster NGC 288, and none have been found in the metal-poor cluster NGC 6093 (however, data are available for only seven BHB stars in this cluster). Both NGC 288 and NGC 6093 have very blue HBs. There is then a clear connection, if not a one-to-one correlation, between rotation and both metallicity and colours along the HB. However, to clarify the meaning of this connection, an explanation for the lack of fast rotators among stars warmer than the Grundahl jump is required (Behr 2003a; Recio-Blanco et al. 2004). For possible suggestions, see Sweigart (2002) and Vink & Cassisi (2002).

3. Analysis

We analysed only the spectra of non-variable stars. Reliable abundances for the RR Lyrae stars would have required scheduled observations taken at appropriate phases; this was not possible for the adopted service mode for the observations.

3.1. Atmospheric parameters

Our analysis is based on model atmospheres extracted by interpolation within the Kurucz (1993) grid, with the overshooting option switched off. Interpolations were made as described in Gratton & Sneden (1987) and as used in many other papers. The grid of models used for this interpolation does not include any enhancement of the α-elements. The effect of α-enhancement, typically observed in metal-poor stars, is expected to be weak for atmospheres with $T_{\rm eff} > 4500$ K (see e.g. Gustafsson et al. 2008). The main effect is expected on the continuum opacity. For RHB stars, opacity is dominated by H^-, with electrons mainly provided by metals. Alpha-enhanced models ([α/Fe] = +0.4) should then resemble α-normal models that are more metal-rich by 0.2–0.3 dex. Given the sensitivity to metal abundance reported below, the effect is minor for almost all species considered in our analysis. The Ba abundances might be systematically underestimated by as much as 0.1 dex, but this effect probably is the same for all stars, so that it does not affect the star-to-star trends considered in this paper. α-enhancement has an even weaker effect on BHB stars, since in this case opacity is mainly due to H, which also contributes most of the free electrons.

The most critical parameter in our abundance analysis is the effective temperature $T_{\rm eff}$. The values we adopted were obtained from the de-reddened $B-V$ colours and, for RHB stars, also from the $V-J$ colours (K magnitudes typically have much larger errors and we prefer not to use them). We used the calibration by Alonso et al. (1999) for the RHB stars, while for the BHB stars we used the same calibration as was adopted for the stars in M 5 by Gratton et al. (2013). The reddening value we adopted is $E(B-V) = 0.05$ from Harris (1996, 2010 edn.). Star-to-star uncertainties in these values for $T_{\rm eff}$ can be obtained by comparing results from different photometric studies. The median of the rms dispersion is 59 K for the BHB stars and 43 K for RHB stars.

Systematic errors are probably larger. We assume that they are about 100 K for RHB stars and twice that for the BHB stars.

Surface gravities were obtained from visual magnitudes and effective temperatures, using the distance modulus $(m-M)_V$ = 14.84 mag from Harris (1996, 2010 edn.), the bolometric corrections by Alonso et al. (1999) for the RHB stars and from Kurucz (1993) for the BHB ones, and masses of 0.610 and 0.664 $M_\odot$ for the BHB and RHB stars. These last values are taken from the Gratton et al. (2010) analysis of the statistical properties of the HB stars. While there are some uncertainties in these adopted quantities, the total errors in the gravities are small (<0.1 dex).

There are too few lines in our spectra for a reliable determination of the microturbulence velocity. We therefore adopted a value of 1.3 km s^{-1} for all RHB stars: this value is intermediate between those adopted for 47 Tuc and M 5 RHB stars in Gratton et al. (2013). For the BHB stars, we used the values given by the relations v_t = 3.0 km s^{-1} for stars with $T_{\rm eff}$ > 9000 K, and v_t = 3.0–0.6($T_{\rm eff}$ −9000) (Gratton et al. 2014), save for star #71676, for which we adopted a lower value of 2.0 km s^{-1} to reach reasonable agreement among different lines of the same element. These values are quite uncertain, mainly for BHB stars, where we deem that the error can be as large as 0.5 km s^{-1} from the scatter found between different BHB studies (compare for instance the values of Marino et al. 2013 with those of For & Sneden 2010). There is much better agreement among different analyses of RHB stars, so that the adopted microturbulence velocities for these stars probably have errors not larger than 0.2 km s^{-1}.

Finally, we adopted a model metal abundance of [A/H] = −1.25, close to the average value we determined for the Fe abundance.

3.2. Equivalent widths

Our abundances rest on measures of equivalent widths (*EW*). In most cases, they were obtained by an automatic procedure analogous to that used in many papers of our team on red giants (see, e.g., Carretta et al. 2009b). The results from this procedure are not accurate for strong lines (*EW* > 150 mÅ). In these cases, the *EW*s were obtained from manual measurements. Since we obtained independent measures from the two spectra obtained with the HR19A set up, we may compare the two values and derive an estimate of the internal error of our *EW*s. The value we obtain (±4.6 mÅ) compares well with that determined using the Cayrel (1988) formula. We estimated internal errors in the *EW*s for the HR12 spectra from comparing results for stars with very similar atmospheric parameters. Since we only used one spectrum per star, the errors are larger (±6.9 mÅ).

3.3. Line list and notes on individual elements

The abundance analysis done in this paper generally follows the scheme outlined in previous papers of this series. In particular, most of the abundances we derived assumed local thermodynamic equilibrium (LTE); however, non-LTE corrections were included for N (Przybilla & Butler 2001; see Gratton et al. 2012b), O (Takeda et al. 1997), and Na (Mashonkina et al. 2000). The He abundances follow the prescriptions in Gratton et al. (2014) and should be considered homogeneous to the non-LTE analysis by Marino et al. (2013).

The only peculiar point concerns the use of only two of the lines in the O I triplet at 7771−75 Å. In fact, we found that in our spectra, the weakest line of the triplet at 7775.4 Å falls very close to a quite strong telluric emission line because of the combination of the cluster velocity and Earth's motion around the barycentre of the solar system (the two observations with HR19 were obtained at short cadence). To avoid uncertain corrections, we preferred to remove this line from our analysis.

Table 6. Sensitivity of abundances on the atmospheric parameters and total errors.

Element	$T_{\rm eff}$ (K)	log g	v_t (km s^{-1})	[A/H]	*EW* (mÅ)	Total
Variation	+100	+0.3	+0.5	+0.2	+10	
			RHB star			
Error	50	0.1	0.2	0.1	5	
[Fe/H] I	0.087	–0.018	–0.120	–0.014	0.027	0.07
[O/Fe] I	–0.208	0.126	–0.045	0.036	0.087	0.12
[Na/Fe] I	0.030	–0.119	0.047	0.042	0.075	0.06
[Mg/Fe] I	–0.037	–0.032	0.048	0.007	0.150	0.08
[Si/Fe] I	–0.051	0.013	0.067	0.017	0.075	0.05
[Ca/Fe] I	0.013	–0.052	0.012	0.018	0.106	0.06
[Ni/Fe] I	0.018	0.021	0.051	0.005	0.087	0.05
[Ba/Fe] II	–0.049	0.093	–0.311	0.077	0.150	0.16
			BHB			
Error	100	0.1	0.5	0.2	5	
[N/Fe] I	0.018	0.049	–0.057	–0.001	0.065	0.07
[O/Fe] I	0.021	–0.002	–0.154	–0.012	0.099	0.16
[Na/Fe] I	0.087	–0.169	–0.057	0.000	0.162	0.13
[Mg/Fe] II	0.000	0.052	–0.056	–0.004	0.144	0.09

3.4. Sensitivity of abundances on the atmospheric parameters

The sensitivity of abundances to the adopted values for the atmospheric parameters is given in Table 6. It was obtained as usual by changing each parameter separately and repeating the abundance analysis. We also considered the contribution to the error due to uncertainties in the equivalent widths, divided by the square root of the typical number of lines used in the analysis. The values were computed for typical uncertainties in each parameter, as determined in Sect. 3.1. Results are given for an RHB and a BHB star.

4. Results

4.1. Metal abundance

Average abundances for BHB and RHB stars are given in Table 9, along with the rms scatter around these mean values. The star-to-star scatter generally agrees fairly well with expectations based on uncertainties in the atmospheric parameters and in the *EW*s, as given in the last column of Table 6. This suggests that most stars share the same chemical composition. The average Fe abundance (only derived for RHB stars) is [Fe/H] = −1.22 ± 0.01 with an rms dispersion for individual stars of 0.07 dex. This error bar only includes the statistical uncertainties; systematic effects are probably stronger (about 0.08 dex) and are mainly dominated by errors in the $T_{\rm eff}$. This value of the Fe abundance agrees well with the literature determinations listed in the Introduction, in particular with the only other high-dispersion study by Fullton & Carney (1996). The α-elements Mg, Si, and Ca are all overabundant, again in agreement with the earlier study by Fullton & Carney (1996).

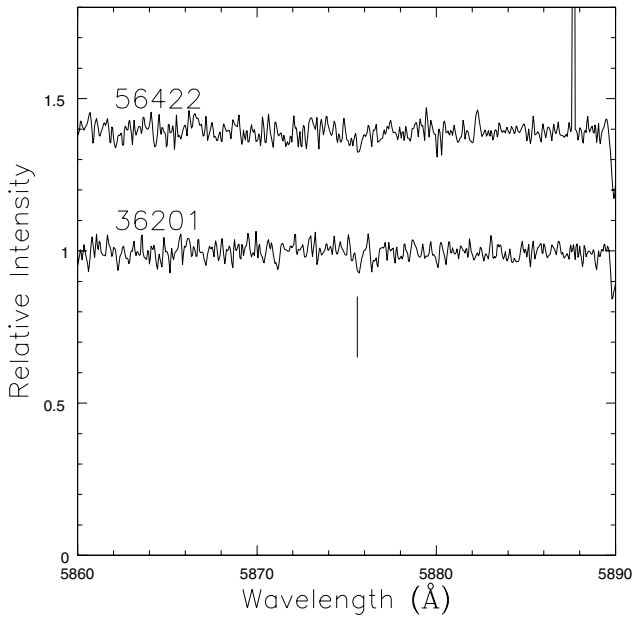

Fig. 4. Spectra in the region of the He I line at 5876 Å for stars #36201 and #56422. Spectra have been offset for clarity.

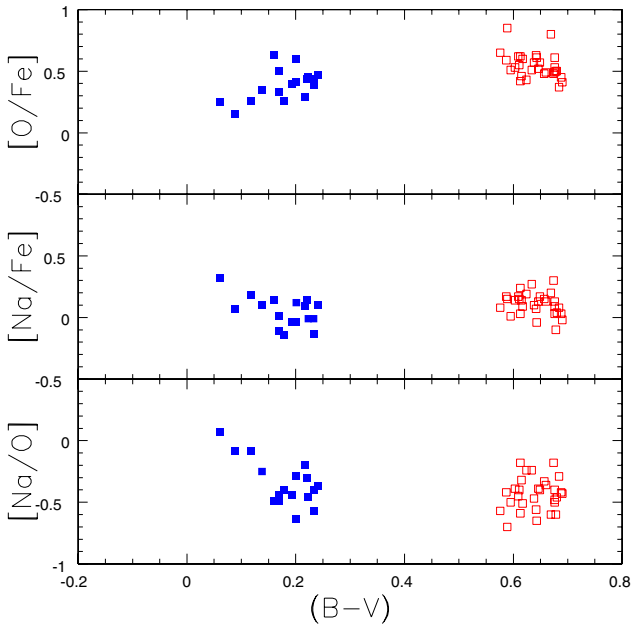

Fig. 5. Run of the [O/Fe] (*upper panel*), [Na/Fe] (*middle panel*), and of the [Na/O] abundance ratios (*lower panel*) as a function of the $B - V$ colour.

Table 9. Average abundances for BHB and RHB stars.

Parameter	BHB	rms	RHB	rms
Y	0.37	0.01	..	..
[Fe/H]	..	..	–1.22	0.07
[N/Fe] I	0.85	0.09	..	..
[O/Fe] I	0.39	0.13	0.53	0.09
[Na/Fe] I	0.05	0.12	0.13	0.09
[Mg/Fe] I	..	..	0.51	0.06
[Mg/Fe] II	0.52	0.08	..	..
[Si/Fe] I	..	..	0.60	0.08
[Ca/Fe] I	..	..	0.81	0.13
[Ni/Fe] I	..	..	–0.01	0.20
[Ba/Fe] II	..	..	0.75	0.17

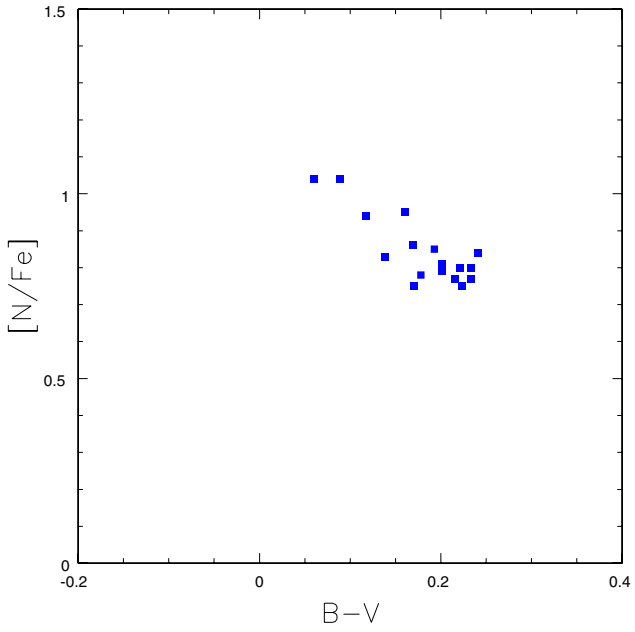

Fig. 6. Run of the N as a function of the $B - V$ colour.

4.2. p-capture elements

For N, O, and Na, all elements whose abundances are affected by p-capture reactions and that are the focus of our analysis, our results indicate that most stars share the same high O and low Na abundances, typical of first generation stars in GCs (Gratton et al. 2012a). This result was expected for the RHB stars; however, almost all BHB stars also share this abundance pattern (see Fig. 5). Only four among the warmest BHB stars are possibly depleted in O and enriched in Na compared to the remaining stars. This evidence is much strengthened by the consideration that these four stars are also enriched in N, with values of [N/Fe] ∼ 1 dex compared to the lower value of [N/Fe] ∼ 0.8 dex observed in the other 13 BHB stars (see Fig. 6). It is interesting to note that these stars are on the bluest and brightest side of a small gap that is possibly visible on the HB of NGC 6723 at $T_{\rm eff}$ ∼ 9000 K (see Fig. 7). While this gap does not appear to be very robust from a statistical point of view (see analysis of possible gaps found in other cases, e.g. Catelan et al. 1998), we used it throughout this paper as a convenient reference point to separate HB stars according to their chemical composition. Whether a real gap is actually present at this this colour or not, we found that there is segregation of first and second generation stars on the HB of NGC 6723 at this colour. This segregation agrees with the hypothesis that the chemical abundances are important factors in determining the distribution of stars along the HB. On the other hand, the wide span in colours ($0.07 < (B - V) < 0.63$) for stars sharing a similar chemical composition suggests that some spread in mass can exist even at constant chemical composition.

4.3. Helium

We tried to measure He abundances for the two warmest stars we observed in NGC 6723 (#36201 and #56422); the remaining stars are too cool to show evidence of helium lines. The method used is described in detail in Gratton et al. (2014). The error bar to be attached is the sum of errors due to atmospheric parameters and equivalent widths; they were obtained by repeating the

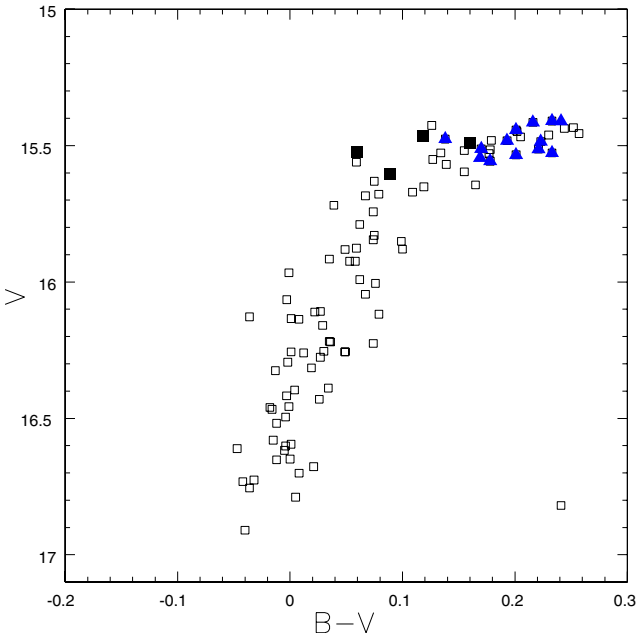

Fig. 7. Zoom on the BHB of NGC 6723; filled symbols are used for O-rich/ Na-poor/N-poor (blue triangles) and O-poor/Na-rich/N-rich stars (black squares). Open squares are for stars not observed in this paper.

analysis with values at the edge of the error bars for these quantities. We obtained very high values of the helium abundance ($Y \sim 0.37$), with similar values derived for both stars. However, the error bar to be attached to these He abundance determinations is large (about ±0.08), given the uncertainties in the *EW*s and in the $T_{\rm eff}$ (these last are larger than usual for these warm stars). The large error bar allows values of the He abundance only slightly higher than the value expected from Big Bang nucleosynthesis ($Y \sim 0.25$: Cyburt 2004) and a modest enrichment due to first dredge-up ($\Delta Y \sim 0.015$: Sweigart 1987). We therefore recommend caution when using these He abundances.

5. Discussion and conclusions

5.1. Comparison with other clusters

We may compare the abundances we obtained for NGC 6723 with those we obtained for other GCs in this series of papers; since the methods are very similar, we expect that the analysis can be considered homogeneous. We may perform a test on the RHB stars, which constitute a more homogeneous sample of stars. In fact, because we expect that when the analysis is limited to stars belonging to the FG, they should have an original He abundance close to that of the Big Bang (Cyburt 2004) and their average effective temperatures should be determined by a combination of metal abundance, age, and mass loss. We observed five clusters with RHB stars: 47 Tuc ([Fe/H] = −0.76; Gratton et al. 2013), M 5 ([Fe/H] = −1.27; Gratton et al. 2013), NGC 1851 ([Fe/H] = −1.18; Gratton et al. 2012b), and NGC 2808 ([Fe/H] = −1.18; Gratton et al. 2011), in addition to NGC 6723 ([Fe/H] = −1.22; this paper). We note that three of these clusters (M 5, NGC 1851 and NGC 2808) are younger than the two others according to Marín-Franch et al. (2009). We also note that all RHB stars in M 5, NGC 1851, and NGC 6723 have compositions compatible with their being FG stars; however, only the reddest stars in 47 Tuc and NGC 2808 are bonafide FG stars, the bluest ones are enriched in Na and depleted in O. Table 10 collects the most important properties of the RHBs of these clusters. Abundances were from this series of papers, where [(Mg, Si)/Fe] is the average of [Mg/Fe] and [Si/Fe] values. Note that we obtained an overall metal abundance by combining the abundances of Fe, Mg, and Si with the rule [M/H] = [Fe/H]+0.25 [(Mg, Si)/Fe][4].

Table 10. Properties of RHB stars.

NGC	[Fe/H]	[(Mg, Si)/Fe]	[M/H]	Relative Age	$\theta_{\rm eff}$(RHB)
104	–0.76	0.26	–0.70	0.99	1.008
1851	–1.18	0.34	–1.10	0.79	0.940
2808	–1.18	0.30	–1.10	0.88	0.925
5904	–1.27	0.24	–1.21	0.86	0.876
6723	–1.22	0.55	–1.08	1.02	0.904

Relative ages are the average of the values obtained by Marín-Franch et al. (2009) using the metallicities reported by Zinn & West (1984) and Carretta & Gratton (1997). Finally, $\theta_{\rm eff}$(RHB) = 5040/$T_{\rm eff}$(RHB), where $T_{\rm eff}$(RHB) is the average temperature for those RHB stars that have the typical composition of FG stars. Although data are available for only five clusters, a bivariate analysis shows a very good correlation between $\theta_{\rm eff}$(RHB) and a combination of [M/H] and age (Pearson linear correlation coefficient of $r = 0.98$). This result does not depend critically on the particular set of ages we adopted for globular clusters; in fact, we derive the same Pearson linear correlation coefficient of $r = 0.98$ when using ages from VandenBerg et al. (2013), for example.

This comparison not only supports our analysis, but also suggests that the FG stars we observed on the BHB of M 5 and NGC 6723 possibly occupy this location on the HB because they lost more mass than normal while evolving along the RGB. This is a possible clue for interpretating of the basic mechanism involved.

The element-to-element abundances agree very well among different clusters for O and Na. NGC 6723 seems to have an excess of α-elements larger than that observed in the other clusters. While this might be related to its greater age, there is no one-to-one correlation between age and excess of α-elements because NGC 1851, the youngest cluster in our sample, is the second-richest in α-elements. The Ca abundances for NGC 6723 are very high. Part of this trend seems to be a systematic effect in our analysis of RHB stars, which systematically produces values of [Ca/Fe] $\sim$ 0.2 dex higher than those obtained from studies of RGB stars (Carretta et al. 2010), and for [Mg/Fe] and [Si/Fe] in the same RHB stars, with a trend for larger differences in warmer stars. Since our Ca abundances are based on rather strong lines with very accurate line data, this difference might be due to non-LTE effects[5]. However, even if corrected for this effect, the [Ca/Fe] ratio found for NGC 6723 stars is still high; this might explain the high metal abundance inferred from applying

[4] This formula is different from that of Straniero & Chieffi (1991); its justification here is simply that it gives a better fit to the data.

[5] Statistical equilibrium computations for neutral calcium lines have been produced by Mashonkina et al. (2007). These authors give non-LTE abundance corrections for one of the lines used in the current analysis (5857 Å), but not for the other one (6122 Å), but they give results for the strongest line of the same multiplet at 6162 Å. Unfortunately, the range of surface gravity they considered does not extend to values appropriate for the RHB, so that some extrapolation would be needed. However, the non-LTE corrections they found are small, and the extrapolations produce values <0.1 dex.

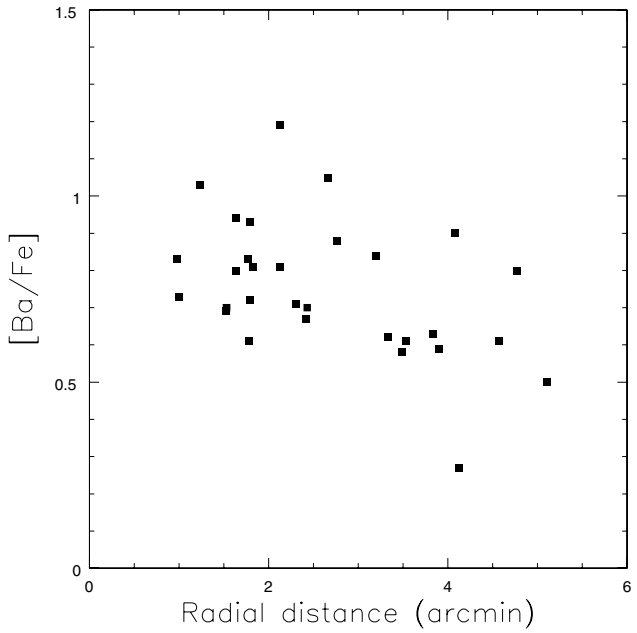

Fig. 8. [Ba/Fe] values as a function of projected distance from center of the cluster.

the ΔS method to the RR Lyrae ([Fe/H] ≈ -0.7: Smith 1981) and the quite high value listed by Zinn & West (1984). A similar suggestion was made by Smith & Hesser (1986).

5.2. Ba abundances

We obtained a very high abundance of Ba in NGC 6723 ([Ba/Fe] = 0.75). Part of this high value can be systematic because we also obtained quite high abundances of Ba for the other clusters we observed. However, when compared with results for RGB stars for the other clusters in this series (Lucatello et al., in prep.), the systematic difference is small, if there is any at all (0.02 ± 0.16). We notice that high abundances of Ba have also been obtained for other moderately metal-rich old GCs: [Ba/Fe] = 0.63, 0.46 and 0.45 for NGC 6121 (=M 4: [Fe/H] = −1.17), NGC 6171 (=M 107: [Fe/H] = −1.03), and NGC 6752 ([Fe/H] = −1.56) (barium abundances are from D'Orazi et al. 2010; Lucatello et al., in prep.; and [Fe/H] values from Carretta et al. 2009b).

However, the most intriguing result we obtained concerning Ba is the correlation between the [Ba/Fe] values and the projected distance from cluster center (see Fig. 8). The Pearson linear correlation coefficient is 0.46 over 30 stars, which has a probability lower than 0.5% to be a random effect. The abundance gradient is not very strong, and RHB stars close to the center of the cluster have Ba abundances that are ∼0.2 dex higher than those at the cluster periphery. This effect is not due to any individual star, and Ba abundances do not correlate with the scatter of radial velocities. There is then no evidence that it is due to mass transfer episodes in close binaries (classical Ba-stars: McClure 1983; McClure & Woodsworth 1990). We found no evidence for radial gradients in the abundances of any other elements, nor any correlation of the Ba abundances with the atmospheric parameters. The Ba abundance gradient seems, then, a real feature of NGC 6723.

Unfortunately, Ba is the only n-capture element we observed. Hence we cannot tell whether this gradient is a consequence of s- or r-processes, which would lead to very different interpretations. Were it due to the r-process, the case could be analogous to that observed in M 15 (Sneden et al. 1997, 2000) and M 92 (Sobeck et al. 2011). The astrophysical site for the r-process is still unknown (see Arnould et al. 2007, for a discussion) with either some special kind of core-collapse supernovae (SNe) (possibly related to gamma-ray bursts: Fujimoto et al. 2008) or merging neutron stars being proposed. The event is probably quite rare to explain the large variance in the abundances of the r-process elements found in extremely metal-poor stars (Gilroy et al. 1988; McWilliam et al. 1995a,b; Roederer et al. 2010) but not too rare to avoid too much a scatter (Argast et al. 2004). Regardless its nature, the event probably occurred within the proto-cluster when it was still very gas-rich and most likely occurred in the central regions, which may explain the radial abundance gradient in Ba observed in NGC 6723. On the other hand, because of the much longer relaxation time, it is more likely that a radial abundance gradient is preserved in NGC 6723 than in M 15. The lowest Ba abundance of NGC 6723 is much higher than that of M 15, requiring a more effective Ba production to produce sizable differences in the Ba abundance; but NGC 6723 is a smaller cluster and the star-to-star variations in Ba abundances are smaller, which at least partly compensates for this difference. Since the total Ba content of NGC 6723 is $\sim 10^{-5}\ M_{\odot}$, this is roughly the amount of Ba that must have been produced by this r-process event (if it was a single episode); note that this is quite a high value for core-collapse SNe (Argast et al. 2004), while it is easily achieved in neutron star mergers (see Argast et al. 2004) and collapsars (Fujimoto et al. 2008). On the other hand, no sizeable abundance difference has been found for elements other than Ba: this limits the total number of SNe that could have exploded in this phase. Since there are $\sim 10\ M_{\odot}$ of O within NGC 6723, the total number of polluting SNe during this phase was probably small, no more than a few (roughly the same numbers also hold for M 15). We note that since in the Sun the Ba/O mass ratio is about 10^{-6}, and about 15% of the solar Ba is due to the r-process (Burris et al. 2000), the Ba/O overproduction does not need necessarily to be extreme. Hence this scenario is well feasible. We finally mention that it is unclear whether applying this scenario to M 15, M 92, and NGC 6723 requires any special connection between the r-process event and GCs. A dedicated search for the spread in the r-process element abundances in GCs might help to clarify this question.

On the other hand, the Ba production required to explain the observed gradient might also be due to the s-process. The main candidate in this case is the main component because we do not have evidence for variations in lighter elements expected from production by the weak component in massive stars. In this case, multiple populations should indeed be present even among the RHB stars of NGC 6723, with age differences so large that pollution is expected to be due to stars too small to have a significant hot bottom burning. The age spread probably is of hundred million years, possibly similar to that proposed to explain the extended turn-off of several intermediate-age clusters in the Magellanic Clouds (Mackey & Broby Nielsen 2007; Milone et al. 2009). However, in this case it appears difficult to avoid variations in the total CNO content and split SGB, such as those observed in NGC 1851 (Milone et al. 2008; Cassisi et al. 2008) and M 22 (Marino et al. 2009). There is no evidence for anything similar in NGC 6723, and we note that there is no radial gradient in N abundances, for instance. However, these arguments are circumstantial and not strong enough to completely discard this hypothesis. Only determination of the abundances for elements with high r-fraction abundances (e.g., Eu) may clarify this question.

We finally add a caveat about the previous discussion: the original mass of globular clusters was certainly higher than the current one, by an amount that is probably different from cluster to cluster and can even be large (see e.g. D'Antona & Caloi 2004; Lamers et al. 2010). All numbers given in this section should therefore be considered with caution and at most as order-of-magnitude estimates. The only conclusion is that at present there is no obvious reason for either an r- or an s-process explanations of the observed scatter in Ba abundances in NGC 6723.

5.3. Distribution of stars along the HB

When discussing our results, we first note that our sample is not exactly representative of the whole HB population of NGC 6723. We may use the photometry by Lee et al. (2014), which extends over the whole cluster, to derive the total number of stars in different portions of the HB. Field contamination is a problem for RHB stars, while we may safely neglect it for the BHB ones. To reduce this concern, we will only used counts of stars within 7.5 arcmin; this limit approximately corresponds to the projected distance from the center of the farthest radial velocity member star in our sample. We have observed 30 RHB stars over a total of about 132; this last total was obtained assuming that the percentage of contaminants is as high in the whole photometric sample as it is in our spectroscopic one within 7.5 arcmin (30 out of 34 our candidate RHB stars within this distance are cluster members). We also observed 4 RR Lyrae stars out of 42; 15 out of 35 BHB stars cooler than the gap that we tentatively found at ~9000 K ($B - V \sim 0.1$), and that may roughly separate the first and second generation along the HB of NGC 6723; and two out of 68 stars warmer than this gap. We note, however, that we also found a N- and Na-excess and an O deficiency for two stars slightly cooler than the possible gap; these stars are slightly brighter than most of the stars with the same colour. Their location on the HB suggests that they are evolved objects that started their HB evolution on the bluer side of the tentative gap. We then combined these stars with the group of stars bluer than the gap. For simplicity we call this last group extreme-BHB below to separate them from the redder stars on the intermediate-BHB that are cooler than this gap.

According to our determinations of the O, Na, and N abundances, RHB and intermediate-BHB stars of NGC 6723 all belong to the first generation because they are O-rich, Na-poor and N-poor. While we have not analysed any of the RR Lyrae stars, we expect that they share the composition of the red and intermediate-BHB stars that bracket them in colours. Hence a total of 132 + 42 + 33 = 207 HB stars belong to the first generation. On the other hand, the only O-poor, Na-rich, and N-rich stars we found in NGC 6723 are the four extreme-BHB stars (these four stars are among the coolest extreme-BHB stars). These are the only stars we observed in NGC 6723 that probably belong to the second generation. Even if we assume that all the extreme-BHB stars belong to the second generation (a reasonable assumption), the total of second-generation stars on the HB of NGC 6723 is 70 stars at most. Although lifetimes of the extreme-BHB stars might be slightly different from those of the remaining HB stars and there is some statistical uncertainty, related in particular to de-contamination of RHB stars from field interlopers, the conclusion that second-generation stars make up at most only a small fraction (70 out of 277, that is, about one fourth) of the total stars of NGC 6723 seems to us straightforward. This low fraction of second-generation stars distinguishes this cluster from many others observed (see, e.g., the compilation by Carretta et al. 2009a) where the second generation usually dominates the first generation and typically makes up some two thirds of the cluster population: normalized to the first generation, the second generation of NGC 6723 is about <1/8 that of a "normal" GC. The large variation of the first-to-second generation ratios indicated by these numbers should provide a caution about, e.g., the use of clusters in the Fornax dwarf galaxy to confirm or dismiss scenarios for internal pollution in GCs (Larsen et al. 2012; Bastian et al. 2013); on the other hand, it should also caution us concerning arguments about the fraction of halo stars that formed in GCs from the population of luminous clusters surveyed so far to the total initial population of globular clusters (Gratton et al. 2012b). We furthermore note that the low central concentration of NGC 6723 may be somehow connected to this peculiarity, although other clusters with a concentration even lower than NGC 6723, such as NGC 288 and NGC 6809, have more normal fractions of FG and SG stars. We finally note that NGC 6723 is not included in the list of clusters suspected to predominantly host FG stars by Caloi & D'Antona (2011).

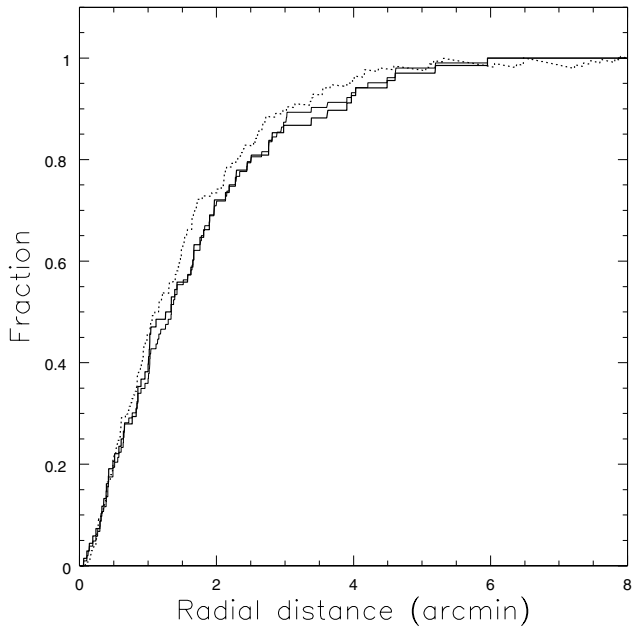

Fig. 9. Cumulative radial distribution for stars on different parts of the HB of NGC 6723. Thin solid line is for stars on the whole BHB, the thick solid line is for stars on the extreme BHB, and the dotted line is for stars on the RHB.

There are several indications that in many clusters second-generation stars are much more centrally concentrated than first-generation stars (see Gratton et al. 2012a). To test this point for NGC 6723, we plot in Fig. 9 the cumulative radial distribution of extreme-BHB stars and compare them with those of other stars on the HB of this cluster. There is no evidence for any difference in the two distributions. On the other hand, we note that NGC 6723 is a cluster with low central concentration, which might be related to the unusual predominance of first-generation stars because FG stars are typically less concentrated than SG stars.

The other interesting fact concerning the HB of NGC 6723 is the wide distribution in colours of first-generation stars. To quantify this spread in colour as a spread in mass and to discuss the relation between first and second generation in NGC 6723, we compared the observed colour-magnitude diagram with synthetic HBs obtained using the same tools as in Gratton et al. (2012b, 2013, 2014) and described in more detail in Salaris et al. (2008) and Dalessandro et al. (2011). We

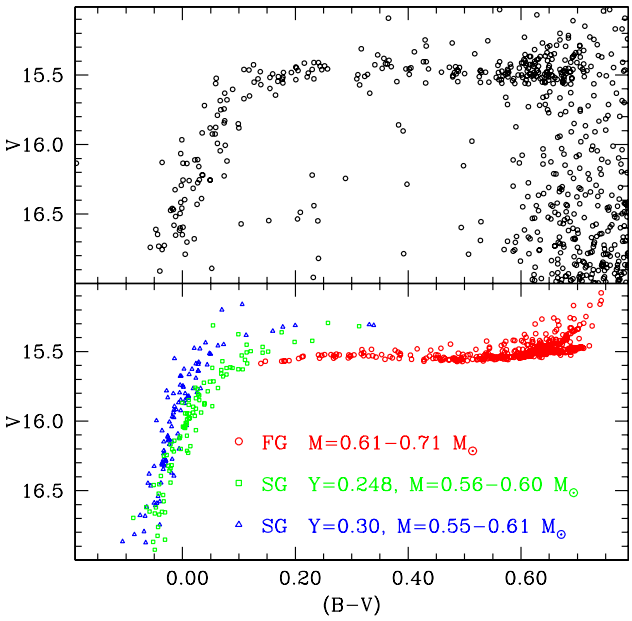

Fig. 10. Comparison between a synthetic (*lower panel*) and an observed (*upper panel*) colour−magnitude diagram for the horizontal branch of NGC 6723. In the lower panel, red circles are FG ($Y = 0.248$) stars (mass range 0.61−0.71 $M_\odot$), while green squares and blue triangles are SG with different values of the He abundance: $Y = 0.248$ and $Y = 0.30$. The mass range for the SG stars is 0.55−0.61 $M_\odot$ in the first case and 0.56−0.60 $M_\odot$ in the second.

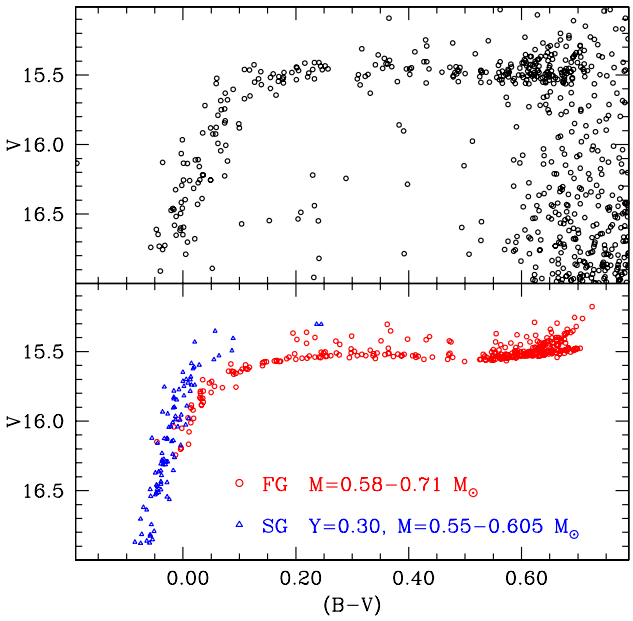

Fig. 11. Same as Fig. 10, but in this case different ranges in mass were adopted: 0.58−0.71 $M_\odot$ for the FG (red open circles) and 0.55−0.605 $M_\odot$ for the SG ($Y = 0.30$) blue open triangles.

used the HB evolutionary tracks with [Fe/H] = −1.25 from the BaSTI database (Pietrinferni et al. 2006), interpolating among the α−enhanced BaSTI models to determine HB tracks for various values of the helium content Y. We adopted a distance modulus $(m - M)_V = 14.84$ and $E(B - V) = 0.05$ from Harris (1996, 2010 edn.). For simplicity, we adopted discrete values for the chemical composition; this assumption is not supported by strong evidence for this particular cluster, but it may be a good approximation for others. However, this assumption is not essential in the following discussion.

We performed several simulations; in all cases we assumed that the helium-rich SG contains one fourth of the stars, as previously discussed. However, this exact value is not crucial here. Figure 10 contains a first comparison. In this case, we assumed that the FG stars (red circles) have a standard Big Bang He abundance ($Y = 0.248$) and a uniform distribution in mass over the range 0.61−0.71 $M_\odot$. Initially, we assumed that SG stars are He-rich ($Y = 0.30$) and have a uniform distribution in mass over the range 0.55−0.61 $M_\odot$ (blue triangles in Fig. 10); this value for Y is close to the lower extreme of the observational range. While the overall range in colours is well covered by this simulation, we note that with such assumptions there is quite a large discontinuity in luminosities (∼0.2 mag) at the transition between the two populations (at $B - V = 0.15$). There is no such obvious discontinuity in the observed data. The discontinuity can be eliminated by assuming a lower He abundance for the SG stars: to show this, we plot in this same figure a synthetic SG computed with the range mass 0.56−0.60 $M_\odot$, but the same value of Y as the FG one ($Y = 0.248$: green squares). However, this value of Y disagrees with the spectroscopic result.

A possible alternative is to assume that SG stars are He-rich, as indicated by spectroscopy, but FG stars have a wider range in masses (0.58−0.71 $M_\odot$). A simulation performed with this assumption is shown in Fig. 11. We also slightly modified the range in mass for the SG to 0.55−0.605 $M_\odot$, but this modification plays a secondary role here. While SG are more luminous than FG stars at the same colour, there is now quite a substantial overlap in colour between the two populations, so that there is no obvious discontinuity at a colour of $B - V = 0.15$. We note that in this simulation, the ratio between the number of RR Lyrae variables and RHB stars is 0.27, close to the observed ratio (42/132), and that the number of FG BHB stars is similar to that of RR Lyraes. This means that a uniform distribution in masses for the FG stars over this wide range is an acceptable approximation. If this interpretation of the HB of NGC 6723 is correct, the ratio between SG and FG stars is even lower than the value of one fourth we concluded in the previous section because some of the extreme BHB stars are FG stars.

We conclude that to reproduce spectroscopic and photometric evidence, the range in mass of FG – that is, of chemically homogeneous – stars in NGC 6723 is probably quite wide: at least 0.10 $M_\odot$, and more likely about 0.13 $M_\odot$. This requires a wide distribution in the mass lost by the stars along the RHB. We recall that a smaller but not negligible spread in mass loss among FG stars was also required to explain the distribution of stars along the HB of M 5 (Gratton et al. 2013). This indicates that at least a fourth parameter (in addition to metallicity, age, and helium abundance) is required to explain the HB of globular clusters, in agreement with earlier suggestions based on other properties of HB stars (see, e.g., the discussion in Catelan 2009).

Acknowledgements. This publication makes use of data products from the Two Micron All Sky Survey, which is a joint project of the University of Massachusetts and the Infrared Processing and Analysis Center/California Institute of Technology, funded by the National Aeronautics and Space Administration and the National Science Foundation. This research has made use of the NASA's Astrophysical Data System. This research has been funded by PRIN INAF "Formation and Early Evolution of Massive Star Clusters". S.L., A.S., E.C., S.C., and A.B. acknowledge financial support from PRIN MIUR 2010−2011, project "The Chemical and Dynamical Evolution of the Milky Way and Local Group Galaxies" (PI F. Matteucci), prot. 2010LY5N2T. V.D. is an ARC Super Science Fellow. We thank Jae-Woo Lee for sending us the full *BV* photometric data they obtained for NGC 6723.

References

Alonso, A., Arribas, S., & Martinez-Roger, C. 1999, A&AS, 140, 261
Argast, D., Samland, M., Thielemann, F.-K., & Qian, Y.-Z. 2004, A&A, 416, 997
Arnould, M., Goriely, S., & Takahashi, K. 2007, Phys. Rep., 450, 97
Bastian, N., Lamers, H. J. G. L. M., de Mink, S. E., et al. 2013, MNRAS, 436, 2398
Bedin, L. R., Piotto, G., Anderson, J., et al. 2004, ApJ, 605, L125
Behr, B. B. 2003a, ApJS, 149, 67
Behr, B.B. 2003b, ApJS, 149, 101
Behr, B. B., Cohen, J. G., McCarthy, J. K., & Djorgowski, S. G. 1999, ApJ, 517, L135
Behr, B. C., Djorgovski, S. G., Cohen, J. G., et al. 2000a, ApJ, 528, 849
Behr, B. C., Cohen, J. G., & McCarthy, J. K. 2000b, ApJ, 531, L37
Burris, D., Pilachowski, C. A., Armandroff, T. E., et al. 2000, ApJ, 544, 302
Caloi, V., & D'Antona, F. 2011, MNRAS, 417, 228
Carretta, E., & Gratton, R. G. 1997, A&AS, 121, 95
Carretta, E., Bragaglia, A., Gratton, R., et al. 2009a, A&A, 505, 117
Carretta, E., Bragaglia, A., Gratton, R., & Lucatello, S. 2009b, A&A, 505, 139
Carretta, E., Bragaglia, A., Gratton, R., et al. 2010, ApJ, 712, L21
Cassisi, S., Salaris, M., Pietrinferni, A., et al. 2008, ApJ, 672, L115
Cassisi, S., Salaris, M., & Pietrinferni, A. 2013, Mem. Soc. Astron. It., 84, 91
Catelan, M. 2009, Ap&SS, 320, 261
Catelan, M., Borissova, J., Sweigart, A. V., & Spassova, N. 1998, ApJ, 494, 265
Catelan, M., Grundahl, F., Sweigart, A. V., Valcarce, A. A. R., & Cortés, C. 2009, ApJ, 695, L97
Cayrel, R. 1988, in The Impact of Very High S/N Spectroscopy on Stellar Physics, eds. G. Cayrel de Strobel, & M. Spite (Dordrecht: Kluwer Academic Publishers), IAU Symp., 132, 345
Cyburt, R. H. 2004, Phys. Rev. D, 70, 023505
Dalessandro, E., Salaris, M., Ferraro, F. R., et al. 2011, MNRAS, 410, 694
D'Antona, F., & Caloi, V. 2004, ApJ, 611, 871
D'Antona, F., Caloi, V., Montalban, J., et al. 2002, A&A, 395, 69
D'Antona, F., Bellazzini, M., Caloi, V., et al. 2005, ApJ, 631, 868
Decressin, T., Meynet, G., Charbonnel, C., Prantzos, N., & Ekström, S. 2007, A&A, 464, 1029
Dinescu, D. I., Girard, T. M., van Altena, W. F., & Lopez, C. E. 2003, AJ, 125, 1373
D'Orazi, V., Gratton, R., Lucatello, S., et al. 2010, ApJ, 719, L213
Dotter, A., Sarajedini, A., Anderson, J., et al. 2010, ApJ, 708, 698
Dotter, A. 2013, Mem. Soc. Astron. It., 84, 97
Faulkner, J. 1966, ApJ, 144, 978
For, B.-Q., & Sneden, C. 2010, AJ, 140, 1694
Fujimoto, S., Nishimura, N., & Hashimoto, M. 2008, ApJ, 680, 1350
Fullton, L. K., & Carney, B. W. 1996, in The Formation of the Galactic Halo...Inside and Out, eds. H. Morrison, & A. Sarajenini, ASP Conf. Ser. (San Francisco, CA: ASP), 92, 256
Fusi Pecci, F., & Bellazzini, M. 1997, in The Third Conference on Faint Blue Stars, eds. A. G. D. Philip, J. Liebert, R. A. Saffer, & D. S. Hayes (L. Davis Press), 255
Geisler, D. 1986, PASP, 98, 847
Gilroy, K. K., Sneden, C., Pilachowski, C. A., & Cowan, J. J. 1988, ApJ, 327, 298
Gratton, R., & Sneden, C. 1987, A&A, 178, 179
Gratton, R. G., Carretta, E., Bragaglia, A., Lucatello, S., & D'Orazi, V. 2010, A&A, 517, A81
Gratton, R. G., Lucatello, S., Carretta, E., et al. 2011, A&A, 534, A123
Gratton, R. G., Carretta, E., & Bragaglia, A. 2012a, A&ARv, 20, 50
Gratton, R. G., Lucatello, S., Carretta, E., et al. 2012b, A&A, 539, A19
Gratton, R. G., Lucatello, S., Sollima, A., et al. 2013, A&A, 549, A41
Gratton, R. G., Lucatello, S., Sollima, A., et al. 2014, A&A, 563, A13
Grundahl, F., Catelan, M., Landsman, W. B., Stetson, P. B., & Andersen, M. I. 1999, ApJ, 524, 242
Gustaffson, B., Edvardsson, B., Eriksson, K., et al. 2008, A&A, 486, 951
Harris, W. E. 1996, AJ, 112, 1487
Hesser, J. E., Shawl, S. J., & Meyer, J. E. 1986, PASP, 98, 403
Kurucz, R. L. 1993, CD-ROM 13 (Cambridge: Smithsonian Astrophysical Observatory)
Lamers, H. J. G. L. M., Baumgardt, H., & Gieles, M. 2010, MNRAS, 409, 305
Larsen, S. S., Strader, J., & Brodie, J. P. 2012, A&A, 544, L14
Lee, J.-W., Lopez-Morales, M., Kyeongsoo, H., et al. 2014, ApJS, 210, 6
Lovisi, L., Mucciarelli, A., Lanzoni, B., et al. 2012, ApJ, 754, L91
Mackey, A. D., & Broby Nielsen, P. 2007, MNRAS, 379, 151
Marín-Franch, A., Aparicio, A., Piotto, G., et al. 2009, ApJ, 694, 1498
Marino, A. F., Milone, A. P., Piotto, G., et al. 2009, A&A, 505, 109
Marino, A. F., Villanova, S., Milone, A. P., et al. 2011, ApJ, 730, L16
Marino, A. F., Milone, A. P., & Lind, K. 2013, ApJ, 768, 27
Mashonkina, I. I., Shimanskii, V. V., & Sakhibullin, N. A. 2000, Astron. Rep., 44, 790
Mashonkina, I. I., Korn, A. J., & Przybilla, N. 2007, A&A, 461, 261
McClure, R. D. 1983, ApJ, 268, 264
McClure, R. D., & Woodsworth, A. W. 1990, ApJ, 352, 709
McWilliam, A., Preston, G. W., Sneden, C., & Searle, L. 1995a, AJ, 109, 2757
McWilliam, A., Preston, G. W., Sneden, C., & Shectman, S. 1995b, AJ, 109, 2736
Milone, A. P., Bedin, L. R., Piotto, G., et al. 2008, ApJ, 673, 241
Milone, A. P., Bedin, L. R., Piotto, G., & Anderson, J. 2009, A&A, 497, 755
Milone, A. P., Piotto, G., Bedin, L. R., et al. 2012, ApJ, 744, 58
Milone, A. P., Marino, A. F., Dotter, A., et al. 2014, ApJ, 785, 21
Norris, J. 2004, ApJ, 612, L25
Norris, J., Cottrell, P. L., Freeman, K. C., & Da Costa, G. S. 1981, ApJ, 244, 205
Pasquini, L., Castillo, R., Dekker, H., et al. 2004, SPIE, 5492, 136
Peterson, R. 1983, ApJ, 275, 737
Pietrinferni, A., Cassisi, S., Salaris, M., et al. 2009, ApJ, 697, 275
Piotto, G., King, I. R., Djorgovski, S. G., et al. 2002, A&A, 391, 945
Piotto, G., Villanova, S., Bedin, L. R., et al. 2005, ApJ, 621, 777
Przybilla, N., & Butler, K. 2001, A&A, 379, 955
Recio-Blanco, A., Piotto, G., Aparicio, A., & Renzini, A. 2004, A&A, 417, 597
Roederer, I. U., Cowan, J. J., Karakas, A. I., et al. 2010, ApJ, 724, 975
Rood, R. T. 1973, ApJ, 184, 815
Rutledge, G. A., Hesser, J. E., Stetson, P. B., et al. 1997, PASP, 109, 883
Salaris, M., Cassisi, S., & Pietrinferni, A. 2008, ApJ, 678, L25
Sandage, A., & Wildey, R. 1967, ApJ, 150, 469
Sarajedini, A., Bedin, L. R., Chaboyer, B., et al. 2007, AJ, 133, 1658
Skrutskie, M. F., Cutri, R. M., Stiening, R., et al. 2006, AJ, 131, 1163
Smith, H. 1981, ApJ, 250, 719
Smith, G. H., & Hesser, J. E. 1986, PASP, 98, 838
Sobeck, J. S., Kraft, R. P., Sneden, C. S., et al. 2011, AJ, 141, 175
Sollima, A., Beccari, G., Ferraro, F. R., et al. 2007, MNRAS, 380, 871
Sneden, C., Kraft, R. P., Shetrone, M. D., et al. 1997, AJ, 114, 1964
Sneden, C., Pilachowski, C. A., & Kraft, R. P. 2000, AJ, 120, 1351
Straniero, O., & Chieffi, A. 1991, ApJS, 76, 525
Sweigart, A. V. 1987, ApJS, 65, 955
Sweigart, A. V. 2002, in Highlights of Astronomy, 12 (ASP), 292
Takeda, Y. 1997, PASJ, 49, 471
VandenBerg, D. A., Brogaard, K., Leaman, R., & Casagrande, L. 2013, ApJ, 775, 134
van den Bergh, S. 1967, AJ, 72, 70
Villanova, S., Piotto, G., & Gratton, R. G. 2009, A&A, 499, 755
Villanova, S., Geisler, D., Piotto, G., & Gratton, R. G. 2012, ApJ, 748, 62
Ventura, P., & D'Antona, F. 2008, A&A, 479, 805
Ventura, P., D'Antona, F., Mazzitelli, I., & Gratton, R. 2001, ApJ, 550, L65
Vink, J. S., & Cassisi, S. 2002, A&A, 392, 553
Zinn, R., & West, M. J. 1984, ApJS, 55, 45

Pages 13 to 16 are available in the electronic edition of the journal at http://www.aanda.org

Table 2. Photometric data.

Star	RA (J2000)	Dec (J2000)	V(Lee)	B(Lee)	V	B	J	H	K
Blue horizontal branch									
36201	284.82925	–36.67456	15.523	15.583	15.508	15.515	15.293	15.282	15.655
36473	284.83075	–36.62700	15.491	15.651	15.459	15.553	15.048	14.885	14.900
37378	284.83563	–36.60417	15.411	15.652	15.401	15.618	14.703	14.589	14.571
44646	284.86296	–36.63647	15.512	15.682	15.483	15.557			
45828	284.86642	–36.65939	15.513	15.734	15.419	15.552	14.840	14.817	14.834
47863	284.87225	–36.59558	15.464	15.582	15.444	15.509	15.047	15.027	14.997
48268	284.87367	–36.61222	15.443	15.644	15.410	15.548	14.707	14.641	14.250
49440	284.87775	–36.61411	15.415	15.631	15.387	15.551			
54070	284.89171	–36.65372	15.485	15.708	15.440	15.628	13.853		
54670	284.89321	–36.65736	15.534	15.735	15.488	15.642	14.719	14.874	14.572
55259	284.89458	–36.66253	15.527	15.760	15.471	15.664	14.808	14.793	14.625
56422	284.89750	–36.67281	15.603	15.692	15.575	15.639	15.344	15.572	15.210
61280	284.91042	–36.60397	15.410	15.643	15.391	15.613			
63763	284.91788	–36.62508	15.476	15.614	15.447	15.559	14.936	14.796	15.111
68779	284.93767	–36.62525	15.557	15.735	15.531	15.694	14.976	14.899	14.869
71676	284.95396	–36.62119	15.482	15.675	15.449	15.646	14.817	14.549	14.569
77469	285.00338	–36.55194	15.545	15.714	15.538	15.684	15.133	15.006	14.829
Red horizontal branch									
32170	284.80267	–36.62553	15.476	16.164	15.474	16.141	14.040	13.594	13.510
34102	284.81654	–36.62303	15.470	16.146	15.467	16.116	13.972	13.617	13.535
34668	284.82046	–36.59639	15.517	16.120	15.526	16.122	14.148	13.795	13.682
41649	284.85346	–36.61975	15.492	16.107	15.473	16.059	14.104	13.737	13.677
42553	284.85642	–36.56922	15.472	16.083	15.488	16.100	14.006	13.659	13.720
42857	284.85738	–36.57339	15.435	16.044	15.447	16.055	14.114	13.749	13.609
43379	284.85917	–36.61406	15.491	16.108	15.479	16.067	14.116	13.691	13.734
44426	284.86242	–36.66694	15.665	16.334	15.530	16.155	14.071	13.646	13.574
46519	284.86829	–36.63739	15.476	16.122	15.456	16.069	13.904		
48528	284.87467	–36.66606	15.525	16.159	15.508	16.122	14.064	13.684	13.653
49317	284.87729	–36.60628	15.495	16.119	15.466	16.076	14.116	13.766	13.764
51670	284.88458	–36.60253	15.452	16.065	15.445	16.044	14.076	13.733	13.629
52012	284.88575	–36.59378	15.491	16.067	15.495	16.073	14.162	13.842	13.917
54960	284.89388	–36.64789	15.538	16.187	15.501	16.126			
56265	284.89708	–36.65158	15.563	16.241	15.503	16.162			
58421	284.90263	–36.67683	15.532	16.208	15.506	16.158	13.992	13.545	13.516
58511	284.90275	–36.55697	15.499	16.094	15.509	16.112	14.123	13.808	13.723
58978	284.90408	–36.61028	15.542	16.216	15.465	16.122			
61405	284.91083	–36.65272	15.512	16.188	15.490	16.153			
61969	284.91246	–36.64842	15.520	16.180	15.496	16.113	14.029	13.664	13.613
63655	284.91750	–36.58208	15.453	16.137	15.462	16.149	13.992	13.571	13.513
65270	284.92308	–36.62197	15.561	16.218	15.493	16.138	14.038	13.674	13.580
65307	284.92325	–36.64167	15.552	16.190	15.537	16.185	14.122	13.745	13.690
65835	284.92513	–36.59936	15.525	16.112	15.522	16.111	14.185	13.862	13.661
66610	284.92804	–36.60747	15.490	16.170	15.477	16.156	14.040	13.651	13.499
67352	284.93121	–36.64028	15.563	16.176	15.544	16.165	14.166	13.821	13.764
71268	284.95133	–36.61556	15.547	16.189	15.535	16.179	14.119	13.754	13.633
72060	284.95654	–36.61092	15.561	16.150	15.560	16.155	14.240	13.872	13.817
75691	284.98592	–36.61997	15.555	16.198	15.560	16.197	14.118	13.769	13.663
75716	284.98604	–36.59953	15.528	16.218	15.533	16.214	13.982	13.598	13.547
RR Lyrae									
45069	284.86417	–36.62147	15.495	15.823					
48493	284.87450	–36.65753	15.392	15.654					
59159	284.90458	–36.64344	15.453	15.807					
68073	284.93433	–36.56781	15.453	15.528					

Table 3. S/N of spectra, radial velocities, FWHM, and rotational velocities.

Star	S/N(12A)	S/N(12B)	S/N(19)	S/N(19B)	RV(12A) (km s^{-1})	RV(12B) (km s^{-1})	RV(19A) (km s^{-1})	RV(19B) (km s^{-1})	⟨RV⟩ (km s^{-1})	rms (Å)	⟨*FWHM*⟩ (Å)	rms (km s^{-1})	$v \sin i$ (km s^{-1})	rms
Blue horizontal branch														
36201	16	40	39	36	–97.19	–96.81	–96.10	–93.67	–95.94	1.58	0.76	0.04	10.4	2.2
36473	21	40	52	53	–92.08	–90.52	–89.96	–90.32	–90.72	0.94	0.69	0.02	5.1	2.1
37378	21	41	53	50	–100.57	–99.13	–99.43	–97.53	–99.17	1.25	0.73	0.03	8.8	1.9
44646	22	30	38	47	–98.73	–96.94	–100.13	–100.72	–99.13	1.68	0.76	0.02	10.2	0.8
45828	22	39	52	42	–92.38	–92.67	–90.58	–92.23	–91.97	0.94	0.67	0.03	<5.0	
47863	24	32	62	43	–102.49	–101.54	–102.48	–100.93	–101.86	0.76	0.65	0.03	<5.0	
48268	25	37	63	43	–92.26	–91.82	–90.63	–92.72	–91.86	0.89	0.69	0.03	5.4	2.4
49440	24	33	53	43	–96.63	–94.99	–95.50	–95.58	–95.67	0.69	0.73	0.01	8.8	0.4
54070	23	40	46	41	–89.98	–90.68	–91.21	–91.06	–90.73	0.55	0.84	0.04	14.3	1.8
54670	14	46	42	48	–93.28	–92.22	–90.66	–91.73	–91.97	1.09	0.73	0.05	8.4	2.7
55259	21	36	55	48	–95.11	–92.78	–92.85	–93.88	–93.66	1.09	0.66	0.03	<5.0	
56422	20	36	41	49	–88.88	–89.84	–88.40	–87.84	–88.74	0.85	0.72	0.04	8.1	2.6
61280	28	31	45	52	–95.57	–95.76	–94.81	–94.36	–95.13	0.65	0.69	0.06	5.9	3.9
63763	18	40	33	35	–97.51	–95.21	–94.63	–97.30	–96.16	1.46	0.66	0.02	<5.0	
68779	20	36	42	40	–95.38	–92.93	–93.20	–96.61	–94.53	1.77	0.64	0.05	<5.0	
71676	26	34	46	38	–94.35	–93.67	–92.13	–95.36	–93.88	1.36	0.66	0.04	<5.0	
77469	26	30	42	40	–95.82	–96.21	–95.94	–95.93	–95.98	0.17	0.64	0.03	<5.0	
Red horizontal branch														
32170	21	34	55	54	–95.32	–94.81	–92.95	–96.42	–94.88	1.45				
34102	21	34	50	62	–100.94	–100.29	–101.36	–102.32	–101.23	0.85				
34668	23	23	59	54	–94.60	–94.88	–93.56	–92.73	–93.94	0.99				
41649	27	33	57	62	–96.71	–95.93	–95.23	–95.82	–95.92	0.61				
42553	20		43	44	–102.77		–100.32	–99.38	–100.83	1.75				
42857	22	35	53	57	–95.64	–95.18	–93.16	–94.40	–94.60	1.09				
43379	22	41	34	36	–98.07	–97.90	–98.23	–96.34	–97.63	0.87				
44426	18	36	63	50	–105.16	–104.73	–104.65	–104.12	–104.67	0.43				
46519	28	48	35	40	–86.41	–84.23	–82.68	–81.90	–83.80	1.99				
48528	22	42	46	39	–94.86	–95.06	–92.48	–94.79	–94.30	1.22				
49317	25	33	52	50	–96.01	–94.97	–93.95	–96.19	–95.28	1.04				
51670	15	33	37	51	–99.88	–98.68	–98.24	–101.39	–99.55	1.41				
52012	22	36	75	48	–105.32	–104.77	–103.39	–103.44	–104.23	0.97				
54960	31	39	56	51	–93.69	–92.94	–92.14	–94.98	–93.44	1.21				
56265	26	33	68	61	–99.95	–99.82	–99.53	–101.21	–100.13	0.74				
58421	26	39	55	52	–97.37	–96.18	–98.75	–98.53	–97.71	1.19				
58511	21	38	61	49	–93.25	–92.84	–91.77	–91.42	–92.32	0.87				
58978	29	35	37	38	–89.61	–88.77	–85.37	–87.76	–87.88	1.83				
61405	27	30	48	50	–96.18	–95.57	–96.51	–97.52	–96.45	0.82				
61969	28	39	50	69	–104.40	–103.55	–104.46	–104.41	–104.21	0.44				
63655	23	44	45	51	–96.84	–96.07	–95.51	–98.79	–96.80	1.43				
65270	24	30	58	62	–99.88	–98.54	–101.84	–96.23	–99.12	2.36				
65307	22	39	45	50	–94.87	–93.99	–96.63	–94.53	–95.00	1.15				
65835	22	31	53	39	–91.06	–90.76	–91.68	–91.53	–91.26	0.42				
66610	23	36	59	51	–98.40	–96.59	–99.14	–99.28	–98.35	1.23				
67352	22	36	62	40	–100.16	–99.88	–100.12	–99.93	–100.02	0.14				
71268	24	46	45	41	–94.83	–94.55	–94.42	–93.67	–94.37	0.49				
72060	23	34	51	38	–91.45	–90.69	–87.47	–91.06	–90.17	1.83				
75691	20	34	47	46	–95.06	–94.15	–96.08	–96.05	–95.34	0.92				
75716	22	36	44	52	–99.91	–98.48	–100.04	–101.62	–100.01	1.28				
RR Lyrae														
45069	26	31	49	47	–109.30	–94.57	–87.04	–88.54	–94.86	10.16				
48493	25	41	64	41	–100.33	–93.77	–100.85	–105.47	–100.10	4.82				
59159	23	29	42	43	–68.49	–81.44	–69.96	–70.15	–72.51	6.00				
68073	27	34	43	48			–67.37	–66.44	–66.90	0.66				

Table 5. Atmospheric parameters.

Star	$T_{\rm eff}$ (K)	Err (K)	$\log g$ (dex)	v_t (km s^{-1})	[A/H] (dex)
Blue horizontal branch					
36201	9312	448	3.32	3.00	–1.25
36473	8308	219	3.17	3.42	–1.25
37378	7711	57	3.03	3.77	–1.25
44646	8070	490	3.13	3.56	–1.25
45828	7997	48	3.09	3.60	–1.25
47863	8652	259	3.21	3.21	–1.25
48268	8037	59	3.10	3.58	–1.25
49440	7930	12	3.07	3.64	–1.25
54070	7849	44	3.07	3.69	–1.25
54670	7995	26	3.12	3.60	–1.25
55259	7807	56	3.08	3.72	–1.25
56422	8847	383	3.29	3.09	–1.25
61280	7721	10	3.03	3.77	–1.25
63763	8324	65	3.16	3.41	–1.25
68779	8032	67	3.15	3.58	–1.25
71676	7904	46	3.09	2.00	–1.25
77469	8104	219	3.16	3.54	–1.25
Red horizontal branch					
32170	5482	75	2.47	1.30	–1.25
34102	5499	33	2.48	1.30	–1.25
34668	5661	50	2.56	1.30	–1.25
41649	5661	51	2.54	1.30	–1.25
42553	5611	69	2.53	1.30	–1.25
42857	5651	25	2.52	1.30	–1.25
43379	5657	46	2.54	1.30	–1.25
44426	5540	50	2.52	1.30	–1.25
46519	5556	67	2.49	1.30	–1.25
48528	5592	29	2.53	1.30	–1.25
49317	5628	5	2.52	1.30	–1.25
51670	5648	33	2.52	1.30	–1.25
52012	5722	81	2.57	1.30	–1.25
54960	5565	25	2.51	1.30	–1.25
56265	5466	13	2.48	1.30	–1.25
58421	5492	26	2.49	1.30	–1.25
58511	5660	64	2.55	1.30	–1.25
58978	5476	9	2.47	1.30	–1.25
61405	5463	0	2.47	1.30	–1.25
61969	5556	49	2.51	1.30	–1.25
63655	5458	78	2.46	1.30	–1.25
65270	5532	19	2.50	1.30	–1.25
65307	5558	41	2.53	1.30	–1.25
65835	5696	62	2.57	1.30	–1.25
66610	5477	79	2.47	1.30	–1.25
67352	5622	38	2.55	1.30	–1.25
71268	5557	31	2.52	1.30	–1.25
72060	5691	53	2.58	1.30	–1.25
75691	5558	12	2.53	1.30	–1.25
75716	5440	44	2.48	1.30	–1.25

Table 7. Abundances for BHB stars.

Star	$EW(Y)$	Y_{NLTE}	[N/Fe]	Err	[O/Fe]	Err	[Na/Fe]	Err	[Mg/Fe]	Err
36201	27.0	0.36	1.04	0.14	0.25	0.16	0.32	0.21	0.62	0.04
36473			0.95	0.14	0.63	0.14	0.14	0.18	0.56	
37378			0.84	0.20	0.47	0.11	0.10	0.25	0.51	0.13
44646			0.75	0.17	0.50	0.03	0.01	0.12	0.47	0.21
45828			0.80	0.17	0.44	0.09	0.14	0.18	0.49	0.06
47863			0.94	0.10	0.26	0.17	0.18	0.01	0.60	
48268			0.81	0.13	0.41	0.14	0.12	0.12	0.47	
49440			0.77	0.20	0.29	0.09	0.09	0.11	0.52	0.27
54070			0.75	0.16	0.45	0.18	–0.01	0.11	0.47	0.26
54670			0.79	0.08	0.60	0.14	–0.04	0.10	0.66	
55259			0.80	0.16	0.39	0.19	–0.01	0.14	0.55	0.02
56422	18.4	0.38	1.04	0.16	0.15	0.09	0.07	0.07	0.64	0.03
61280			0.77	0.11	0.44	0.12	–0.13	0.05	0.32	
63763			0.83	0.17	0.35	0.21	0.10	0.07	0.42	
68779			0.78	0.15	0.26	0.10	–0.14	0.13	0.57	0.03
71676			0.85	0.13	0.40	0.19	–0.04	0.07	0.52	
77469			0.86	0.13	0.33	0.13	–0.11	0.09	0.49	0.19

Table 8. Abundances for RHB stars.

Star	[Fe/H]	Err	[O/Fe]	Err	[Na/Fe]	Err	[Mg/Fe]	[Si/Fe]	Err	[Ca/Fe]	[Ni/Fe]	[Ba/Fe]
32170	–1.11	0.24	0.45	0.12	0.03	0.11	0.59	0.45	0.09	0.78	0.18	0.27
34102	–1.22	0.22	0.53	0.10	0.03	0.11	0.54	0.51	0.04	0.69	–0.09	0.58
34668	–1.26	0.24	0.53	0.05	0.14	0.15	0.52	0.63	0.09	0.81	0.26	0.59
41649	–1.23	0.22	0.46	0.02	0.14	0.07	0.55	0.64	0.09	0.85	–0.13	0.81
42553	–1.34	0.20	0.55	0.09	0.15	0.05	0.60	0.70	0.09	0.70		0.90
42857	–1.25	0.20	0.62	0.16	0.17	0.13	0.53	0.48	0.09	0.82		0.63
43379	–1.21	0.21	0.60	0.03	0.09	0.15	0.44	0.64	0.13	0.50	–0.06	0.83
44426	–1.08	0.19	0.80	0.14	0.20	0.12	0.50	0.58	0.11	0.69	–0.27	0.67
46519	–1.19	0.18	0.52	0.13	0.13	0.06	0.47	0.50	0.08	0.77	–0.18	0.73
48528	–1.18	0.23	0.51	0.04	0.27	0.04	0.44	0.62	0.09	0.86	–0.17	0.81
49317	–1.26	0.12	0.43	0.10	0.19	0.15	0.55	0.72	0.07	1.04	–0.13	0.94
51670	–1.21	0.15	0.42	0.08	0.24	0.13	0.36	0.57	0.13	0.89	–0.27	0.93
52012	–1.23	0.23	0.65	0.08	0.08	0.26		0.60	0.12	0.99		0.71
54960	–1.20	0.24	0.57	0.20	0.17	0.13	0.53	0.55	0.11	0.90	–0.04	0.83
56265	–1.35	0.19	0.50	0.06	–0.10	0.03	0.58	0.49	0.10	0.76	0.23	1.03
58421	–1.18	0.19	0.61	0.18	0.13	0.05	0.46	0.55	0.04	0.78	0.07	0.88
58511	–1.28	0.22	0.51	0.14	0.01	0.17	0.49	0.64	0.08	0.70		0.61
58978	–1.19	0.16	0.48	0.12	0.30	0.07	0.54	0.57	0.14	0.67	–0.33	0.70
61405	–1.17	0.18	0.49	0.14	0.09	0.10	0.52	0.62	0.06	0.90	0.18	0.80
61969	–1.31	0.12	0.49	0.14	0.13	0.09	0.54	0.73	0.09	0.87	0.25	0.69
63655	–1.10	0.25	0.37	0.07	0.08	0.04	0.44	0.59	0.05	0.70	0.04	0.62
65270	–1.31	0.18	0.48	0.14	0.15	0.05	0.56	0.64	0.15	0.72		0.72
65307	–1.19	0.20	0.57	0.05	0.10	0.07	0.48	0.63	0.10	0.91	–0.03	0.61
65835	–1.31	0.14	0.59	0.17	0.17	0.23	0.58	0.69	0.17	1.06	0.35	1.05
66610	–1.14	0.18	0.50	0.08	0.04	0.07	0.44	0.51	0.04	0.75	0.08	0.70
67352	–1.28	0.17	0.62	0.11	0.03	0.15	0.48	0.62	0.21	0.70	0.14	1.19
71268	–1.21	0.15	0.63	0.11	0.07	0.06	0.52	0.61	0.05	0.83		0.84
72060	–1.21	0.26	0.85	0.15	0.15	0.19	0.37	0.56	0.04	0.99	0.06	0.61
75691	–1.41	0.28	0.61	0.03	–0.04	0.21	0.54	0.53	0.10	0.82	0.18	0.80
75716	–1.13	0.23	0.41	0.08	–0.02	0.09	0.37	0.57	0.14	0.74	0.05	0.50